Uranium Exerts Acute Toxicity by Binding to Pyrroloquinoline Quinone Cofactor

MICHAEL R. VANENGELEN,[†,‡] ROBERT K. SZILAGYI,[§] ROBIN GERLACH,[†,‡] BRADY D. LEE,[∥] WILLIAM A. APEL,[∥] AND BRENT M. PEYTON*[,†,‡]

Department of Chemical and Biological Engineering, Montana State University, Bozeman, Montana 59717-3920, United States, Center for Biofilm Engineering, Montana State University, Bozeman, Montana 59717-3980, United States, Department of Chemistry and Biochemistry, Montana State University, Bozeman, Montana 59717, United States, and Biological Systems Department, Idaho National Laboratory, Idaho Falls, Idaho 83415, United States

Received May 24, 2010. Revised manuscript received September 2, 2010. Accepted September 8, 2010.

Uranium as an environmental contaminant has been shown to be toxic to eukaryotes and prokaryotes; however, no specific mechanisms of uranium toxicity have been proposed so far. Here a combination of in vivo, in vitro, and in silico studies are presented describing direct inhibition of pyrroloquinoline quinone (PQQ)-dependent growth and metabolism by uranyl cations. Electrospray-ionization mass spectroscopy, UV−vis optical spectroscopy, competitive Ca^{2+}/uranyl binding studies, relevant crystal structures, and molecular modeling unequivocally indicate the preferred binding of uranyl simultaneously to the carboxyl oxygen, pyridine nitrogen, and quinone oxygen of the PQQ molecule. The observed toxicity patterns are consistent with the biotic ligand model of acute metal toxicity. In addition to the environmental implications, this work represents the first proposed molecular mechanism of uranium toxicity in bacteria, and has relevance for uranium toxicity in many living systems.

Introduction

The global distribution of uranium (U) contamination has remained a persistent environmental and human health problem for several decades. U contamination is the result of a number of activities including U mining (*1*), the production and use of depleted U for military purposes (*2*, *3*), and from legacy wastes generated during development of nuclear weaponry (*4*). The impact of bacteria and bacterial metabolism on U fate and transport has received considerable attention, particularly to the extent that microbial processes can be employed in U bioremediation. These processes include reduction of U(VI) to less soluble and less toxic U(IV) (*5*), and accumulation within biomass (*6*). Although U is known to be toxic to microorganisms, mechanisms of U toxicity are yet to be defined despite the importance of U-bacterial interactions on U fate and mobility.

Webb et al. reported inhibition of Mn(II) oxidation by *Bacillus* sp. strain SG-1 in the presence of only 4 μM UO_2^{2+} (*7*) and more recently suggested that UO_2^{2+} might slow Mn(II) oxidation possibly by inhibiting the Mn(II)-oxidizing enzyme (*8*). It has been recently suggested that pyrroloquinoline quinone cofactor (PQQ, Figure 1a) is involved in bacterial Mn(II) oxidation, based on in vitro studies with the Mn(II) oxidizing marine organism *Erythrobacter* sp. strain SD21 (*9*). PQQ is a noncovalently bound *ortho*-quinone cofactor of a number of bacterial dehydrogenases (*10*). Biogenic manganese oxides have been shown to have high heavy-metal binding capacities (*11*) and are therefore believed to play an important role in hexavalent dioxo-uranium cation, UO_2^{2+} or uranyl mobility, particularly in oxic groundwater environments where UO_2^{2+} mobility is controlled by adsorption onto mineral surfaces (*12*).

Although the role of PQQ in nonbacterial organisms is still debated (*13*, *14*), positively identifying the UO_2^{2+} binding site on PQQ has implications for understanding UO_2^{2+} toxicity in other organisms, including humans. In particular, the ability of UO_2^{2+} to bind to a pyridine nitrogen and quinone oxygen structural motif separated by two atoms may render UO_2^{2+} as a potential inhibitor of flavoproteins. Flavoproteins have at their catalytic center a tricyclic alloxazine group (Figure 1b), which offers a similar coordination environment to UO_2^{2+}. Interestingly, a previous report stated that UO_2^{2+} can exert "remarkable" inhibition of flavoprotein monoamineoxidase (MAO) from renal rat kidney (*15*).

This report presents in vivo, in vitro, and in silico studies that demonstrate the inhibition of microbial activity by UO_2^{2+} at micromolar concentrations upon binding to PQQ. The data presented here show that UO_2^{2+} selectively binds at the carboxyl oxygen, pyridine nitrogen, and quinone oxygen in C7, N6, C5 positions ([ONO] coordination site, Figure 1a), respectively. This site is known to be occupied by a Ca^{2+} ion serving both catalytic (*16*) and structural roles by anchoring the PQQ within the holoenzyme (*17*).

Experimental Proceedures

In Vivo Experiments. The *Pseudomonas aeruginosa* PAO1 strain used in this study was provided by Dr. Michael Franklin (Montana State University, Bozeman, MT). Growth medium composition was as described elsewhere (*18*). Cells were grown aerobically at pH 7.0, 20 °C, and in 125 mL serum bottles sealed with butyl rubber stoppers and crimped with Al seals. Carbon sources were added to a concentration of 25 mM carbon. Data points correspond to the average of either triplicate or duplicate measurements, and reported errors correspond to 95% confidence intervals.

In Vitro Experiments. Absorbance data and spectra were measured using a Thermo Electron Multiskan Spectrum UV−vis spectrophotometer. Mass spectra were collected using an electrospray-ionization mass spectrometer (Agilent Ion Trap 6300, model G2440DA). All compounds and mixtures were infused, immediately after mixing, at a concentration

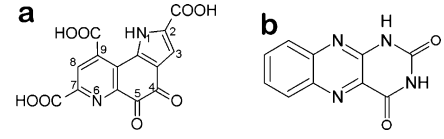

FIGURE 1. Chemical structure of the pyrroloquinoline quinone (PQQ) cofactor (a) and alloxazine (b).

* Corresponding author. E-mail: bpeyton@coe.montana.edu.
† Department of Chemical and Biological Engineering, Montana State University.
‡ Center for Biofilm Engineering, Montana State University.
§ Department of Chemistry and Biochemistry, Montana State University.
∥ Idaho National Laboratory.

10.1021/es101754x
Published on Web 12/17/2010

of 10 μM in nanopure (17.5 MΩ) water as solvent at a flow rate of 0.3 mL/h. PQQ was added as the disodium salt (Sigma-Aldrich, St. Louis, MO), UO_2^{2+} and Ca^{2+} as chloride salts (International Bio-Analytical Industries Inc., Boca Raton, FL and Fisher Scientific, Fair Lawn, NJ, respectively). Nitrogen served as nebulizing and drying gas at a flow rate of 8.0 L/min, 365 °C, and 75 psi. All spectra were obtained in negative mode. Ethanol concentrations were measured using a Hewlett-Packard 5890 series II gas chromatograph according to Wu et al. (*19*).

In Silico Experiments. Geometric structural optimizations were carried out using density functional theory (BP86) (*20, 21*) with relativistically corrected effective core potentials (LANL2DZ) (*22, 23*) for all atoms. All structural minima were confirmed to be stationary points by vibrational analysis. To approximate the aqueous solvent environment of the uranyl complexes, simulations were also carried out in a polarizable solvent environment (*24, 25*) with water solvent parameters (dielectric constant of 80, solvent radius 1.38 Å) as implemented in Gaussian 03 (*26*). The calculations involving the truncated PQQ ligand were done for gas phase conditions.

Results and Discussion

In Vivo Studies: UO_2^{2+}-Induced Inhibition of PQQ-Dependent Ethanol Metabolism. *Pseudomonas* spp. oxidize ethanol under aerobic conditions using a periplasmic PQQ-dependent quinoprotein ethanol dehydrogenase (QEDH) (*27*). This ethanol oxidation step has importance in vivo for both energy production and cell component synthesis. Oxidation is believed to proceed via a hydride transfer mechanism to the PQQ cofactor (*28*), producing reduced $PQQH_2$ and acetaldehyde (*29*).

As shown in Figure 2a, low micromolar concentrations of UO_2^{2+} significantly inhibited aerobic growth of *Pseudomonas aeruginosa* PAO1 on ethanol as the sole carbon and energy source. PAO1, when grown on ethanol was significantly inhibited by 0.5 μM UO_2^{2+} (added as UO_2Cl_2 in nanopure water), which is only about four times the U.S. Environmental Protection Agency drinking water standard of 0.126 μM. The 0.5 and 1 μM UO_2^{2+} concentrations extended the lag phase by 8 and 17 h, respectively. It is worth noting that the UO_2^{2+} only affected the lag phase and not the growth rates, possibly indicating that the bioavailability of the UO_2^{2+} had diminished to the point of losing its toxic influence. Parallel inhibition studies of ethanol oxidation suggest that QEDH is a target of UO_2^{2+} binding. UO_2^{2+} inhibition of ethanol oxidation by PAO1 was measured directly by comparing ethanol consumption rates of PAO1 cultures under nongrowth conditions. In the absence of UO_2^{2+}, PAO1 completely consumed 7.5 mM of ethanol within 23 h, corresponding to an ethanol consumption rate of 0.021 ± 0.001 mmol EtOH h^{-1} (mg protein)$^{-1}$. The presence of 20 μM UO_2^{2+} almost completely inhibited ethanol oxidation, with 87 ± 4% of the ethanol originally present still detected after 47 h of periodic sampling (compared to 92 ± 4% in the cell free control). This further supports the ability of UO_2^{2+} to significantly inhibit the activity of the QEDH enzyme. In contrast, with dextrose as the sole carbon source in a control experiment for non PQQ-dependent growth conditions, PAO1 tolerated UO_2^{2+} concentrations of 25 μM without significant inhibition, thus showing a more than 50-fold increase in UO_2^{2+} tolerance (Figure 2b).

The relationship between PQQ-dependent growth conditions and acute UO_2^{2+} toxicity shown here is in agreement with a recent study with an environmental *Pseudomonas* sp. bacterium isolated from soil cores collected from the Idaho National Laboratory (INL) (Idaho Falls, ID) (*18*). This isolate was inhibited by submicromolar UO_2^{2+} concentrations during aerobic growth on ethanol. Aerobic growth on dextrose, lactate, or butyrate decreased UO_2^{2+} toxicity more than 2 orders of magnitude. It was hypothesized that the acute UO_2^{2+} toxicity was related to PQQ-dependent growth, and that this dependence was a result of UO_2^{2+} binding directly to PQQ.

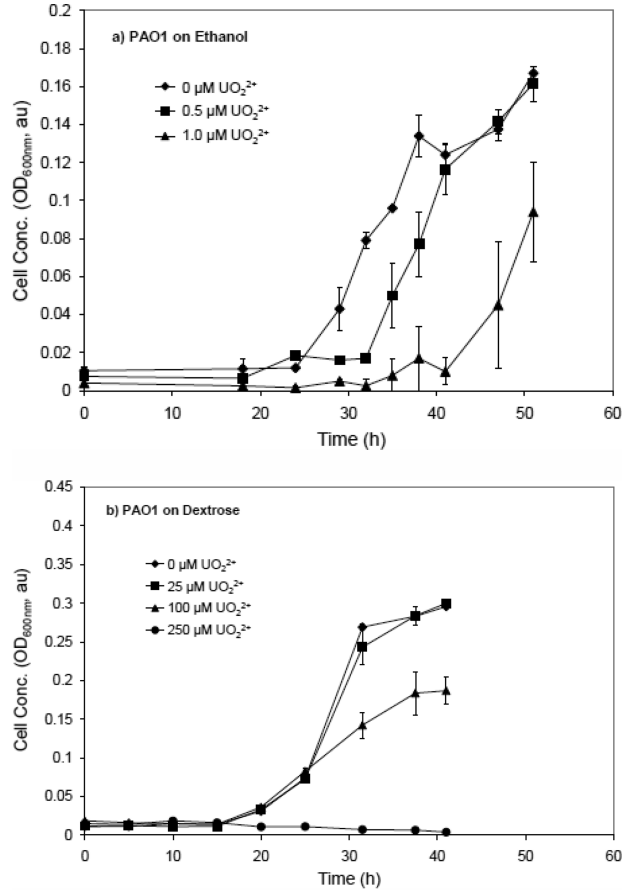

FIGURE 2. In vivo studies of growth of *Pseudomonas aeruginosa* PAO1 on ethanol (a) and dextrose (b) in the presence of UO_2^{2+}. Data points correspond to averages of triplicate measurements. Error bars correspond to 95% confidence intervals.

In Vitro Studies: Direct Evidence of UO_2^{2+}-PQQ Binding. The ability of UO_2^{2+} to bind to PQQ was studied directly using UV−vis spectroscopy and electrospray ionization mass spectroscopy (ESI-MS). UV−vis spectra of PQQ and its complexes with Ca^{2+} and UO_2^{2+} are shown in Figure 3a. The spectrum of a 1.0 mM PQQ solution displays a very broad peak around 460 nm. Addition of equimolar Ca^{2+} (added as $CaCl_2$ in nanopure water) shifts this peak to slightly longer wavelengths due to the emerging interaction between the Ca^{2+} and the quinone oxygen in C5 position (*30*). However, the addition of an equimolar amount of UO_2^{2+} altered the spectrum dramatically. The broad peak centered at 460 nm disappeared, and absorbance at shorter wavelengths increased considerably. The absorbances of the metal-only solutions were undetectable, and therefore their spectra were not included. Visually, the addition of UO_2^{2+} caused the PQQ solution to turn from a brick red color to a brilliant yellow. A similar spectrum was observed when UO_2^{2+} was added to a mixture of PQQ and Ca^{2+}, suggesting that UO_2^{2+} preferentially binds to PQQ over Ca^{2+}. The spectral changes observed here are consistent with changes recently reported by Dimitrijevic et al. for PQQ binding to coordinatively unsaturated Ti(IV) species on the surface of nanocrystalline TiO_2 particles (*31*). From the same study, changes in IR spectra between free PQQ and Ti(IV)-coordinated PQQ provided evidence that Ti(IV) binds to the PQQ at the carboxyl oxygen, pyridine nitrogen, and quinone oxygen in C7, N6, and C5 positions, respectively. Specifically, the C═O quinone car-

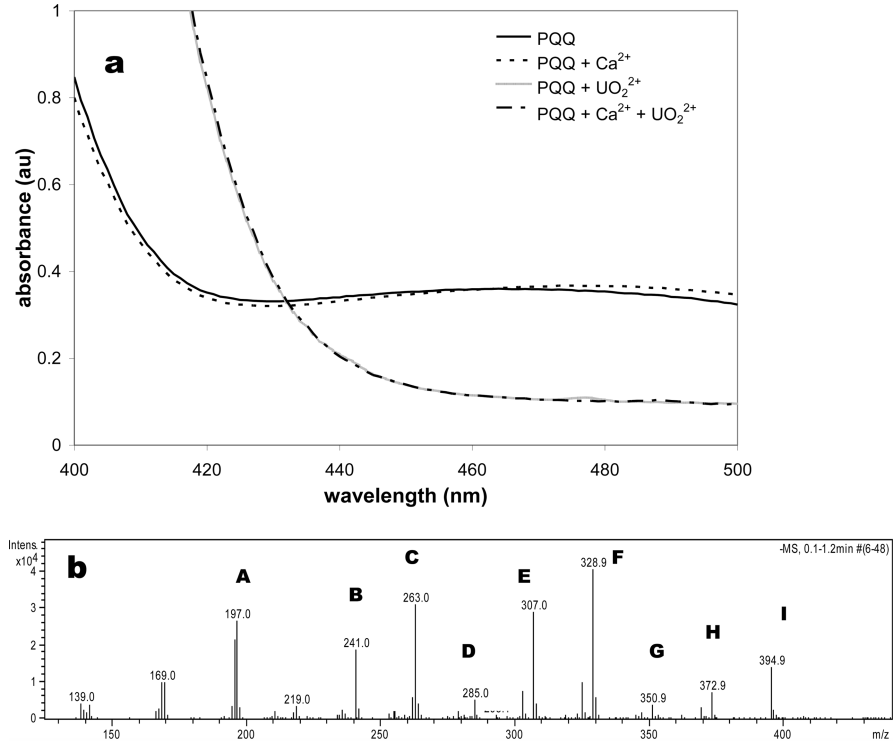

FIGURE 3. In vitro measurements for complexation of PQQ and UO_2^{2+}. UV−vis absorbance spectra (a) of PQQ and its complexes with Ca^{2+} and UO_2^{2+}. The reference mass spectrum (b) of PQQ and PQQ complexes with Ca^{2+} and UO_2^{2+} with prominent peaks A-I. The *m/z* values for PQQ + Ca^{2+}, PQQ + UO_2^{2+}, and PQQ + Ca^{2+} + UO_2^{2+} mass spectra are listed in Table 1.

TABLE 1. Peak Assignments of PQQ and PQQ Complexes with Ca^{2+} and UO_2^{2+} According to Figure 3b[a]

	PQQ		PQQ + Ca^{2+}		PQQ + UO_{22+}		PQQ+Ca^{2+}+UO_{22+}	
	m/z	species	*m/z*	species	*m/z*	species	*m/z*	species
A	197	PQQ − $3CO_2$ − H^+			527	A + UO_2CO_3	527	A + UO_2CO_3
B	241	PQQ − $2CO_2$ − H^+	241	B	571	B + UO_2CO_3	571	B + UO_2CO_3
C	263	PQQ − $2CO_2$ − $2H^+$ + Na^+	263	C	593	C + UO_2CO_3	593	C + UO_2CO_3
D	285	PQQ − CO_2 − H^+	323	D − $2H^+$ + Ca^{2+}	615	D + UO_2CO_3		
E	307	PQQ − CO_2 − $2H^+$ + Na^+	345	E − $2H^+$ + Ca^{2+}	637	E + UO_2CO_3	637	E + UO_2CO_3
F	329	PQQ − H^+	367	F − $2H^+$ + Ca^{2+}	659	F + UO_2CO_3	659	F + UO_2CO_3
G	351	PQQ − $2H^+$ + Na^+	351	G	351	G	351	G
H	373	PQQ − $3H^+$ + $2Na^+$	373	H	373	H	373	H
I	395	PQQ − $4H^+$ + $3Na^+$	395	I	395	I	395	I

[a] The left column contains the *m/z* value and speciation of each fragment in the PQQ only system. The three right columns summarize the peaks obtained when PQQ is equilibrated with Ca^{2+}, UO_2^{2+}, or both metals.

bonyl band of the free PQQ (1643 cm^{-1}) was split, producing bands at 1653 cm^{-1} and 1636 cm^{-1}, indicating an interaction between Ti(IV) and PQQ oxygen at the C5 position. The C═O ester band at 1744 cm^{-1} of the free PQQ was decreased in intensity and shifted to 1749 cm^{-1}, indicating an interaction between Ti(IV) and PQQ oxygen at the C7 position.

In addition to optical spectroscopic techniques, the PQQ-UO_2^{2+} complex was further investigated by ESI-MS in negative detection mode. Figure 3b shows a spectrum of a 10 μM PQQ solution in water (pH 7.0) and a summary of peak assignments (labeled A to I with increasing m/z values). The tallest peak (F) at m/z = 329 corresponds to the deprotonated PQQ molecule. Consistent with previous results (*32*), the PQQ fragmented through the consequential loss of carboxyl groups as CO_2 giving rise to peaks m/z = 285 (peak D), 241 (peak B), and 197 (peak A). Since PQQ was added as the disodium salt, sodium adducts also appear in the spectrum at m/z = 263, 307, 351, 373, and 395 (peaks C, E, G, H, and I, respectively, assignments are given in Table 1). These nine peaks produced by PQQ provided a fingerprint, which was compared to spectra generated by PQQ complexes with either Ca^{2+} or UO_2^{2+} or both being present. An equimolar mixture of PQQ and Ca^{2+} produced a spectrum with five peaks in common with the PQQ-only spectrum, including those labeled B, C, G, H, and I. However, Table 1 shows three peaks at m/z = 323, 345, and 367 unique to the PQQ + Ca^{2+} spectrum, and corresponding PQQ-Ca^{2+} complexes formed between Ca^{2+} and intact PQQ (peak F) and two singly decarboxylated PQQ species (peaks D and E). Adding UO_2^{2+} produced a spectrum with three peaks in common with the PQQ-only and PQQ + Ca^{2+} spectra, including G, H, and I. The remaining six peaks were unique to the PQQ + UO_2^{2+} system. These had the same spacing pattern as peaks A-F of the PQQ spectrum, but were shifted by 330 m/z units. This suggested that UO_2^{2+} remained bound to PQQ, and specifically that UO_2^{2+} was binding as the neutrally charged uranyl bicarbonate complex (UO_2CO_3, M_w = 330 g/mol). Uranyl carbonates are expected to form in aqueous systems open to the atmosphere (*33*).

Potential binding sites included any of the three carboxyl groups, as UO_2^{2+} is known to have an affinity for such a coordination environment (*34*), the quinone oxygens, and

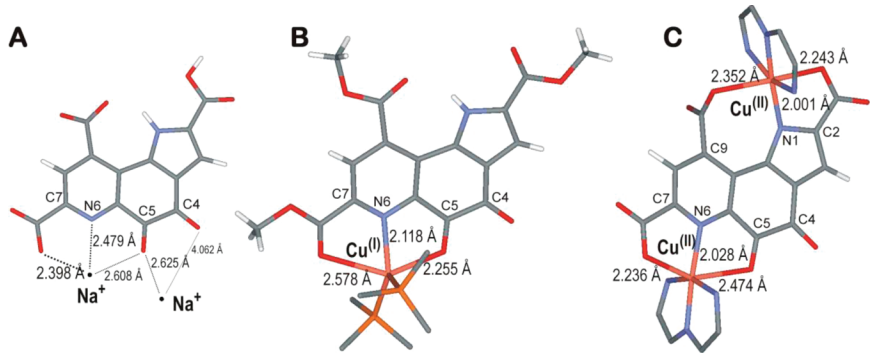

FIGURE 4. Experimental structures with selected bond lengths from the Cambridge Crystallographic Database (*35*) of disodium salt of the PQQ ligand (a) (*36*), tri-O-methylated PQQ coordinated to Cu(I)$(PPh_3)_2$ (b) (phenyl rings of the phosphine ligands were omitted for clarity), and di-Cu(II) (terpyridine) coordinated PQQ (c) (pyridine rings of the terpyridine were omitted for clarity) (*38*).

the Ca^{2+} binding site (*16, 17*). In addition to providing insight into the speciation of the bound UO_2^{2+}, the PQQ + UO_2^{2+} spectrum also narrowed the possible UO_2^{2+} binding sites to two, either the two quinone oxygens or the Ca^{2+} binding site. The peak at $m/z = 527$ of the PQQ + UO_2^{2+} spectrum resulted from UO_2CO_3 binding to the completely decarboxylated PQQ fragment A, thus ruling out the carboxyl groups as the preferred binding sites. Evidence supporting UO_2^{2+} binding at the Ca^{2+} binding site was obtained from the ESI-MS data for a mixture of 10 μM each of PQQ, Ca^{2+}, and UO_2^{2+}. Five peaks corresponding to PQQ + UO_2CO_3 complexes appeared in this spectrum without the presence of any peaks for the PQQ + Ca^{2+} complexes. These observations corroborate the above UV−vis data in suggesting that UO_2^{2+} preferentially binds to PQQ over Ca^{2+}, even in the formally neutral uranyl bicarbonate form. The UO_2^{2+} therefore binds to PQQ via the pyridine nitrogen and/or quinone oxygen in N6 and C5 positions, respectively.

In Silico Studies: Structure and Stability of UO_2^{2+}-PQQ Complex. To obtain further evidence for the likely binding site of UO_2^{2+} on PQQ, relevant crystal structures were reviewed using the Cambridge Crystallographic Database (CCDB) (*35*). The structure of the disodium salt of the uncoordinated PQQ has been determined (Figure 4a, Na_2PQQ) with deprotonated carboxylates in positions C7 and C9 (*36*). The location of the closest counterion to the PQQ^{2-} ligand indicates that the carboxyl oxygen, pyridine nitrogen, and quinone oxygen in C7, N6, C5 positions, respectively, form a preferred nucleophilic binding pocket for cations. Even when the carboxyl groups are alkylated, a $(PPh_3)_2Cu^{(I)}$ cationic moiety coordinates similarly to the cation binding pocket (Figure 4b, [$(PPh_3)_2Cu^{(I)}$](PQQ)) (*37*). If deprotonated, the pyrrole nitrogen in position N1 allows the formation of two metal binding sites (Figure 4c, [(tpy)$Cu^{(II)}$](PQQ)) as two $Cu^{(II)}$(terpyridine) cationic moieties coordinate at the opposite sides of PQQ in positions C5, N6, C7 and C9, N1, C2 ([ONO]- and [ON'O]-coordination, respectively) (*38*).

To further substantiate the preference of UO_2^{2+} binding to the [ONO] motif in positions C5, N6, and C7, in silico studies were performed using density functional theory with a realistic solvent environment. In addition, the effect of protonation state of PQQ and coordination environment of UO_2^{2+} was also evaluated. Table 2 summarizes the calculated thermodynamic parameters and Figure 5 shows representative optimized molecular structures for the most relevant coordination models of UO_2^{2+}. For brevity, with respect to UO_2^{2+}coordination, only the two extreme cases of protonation states for the PQQ ligand are reported here. The fully protonated PQQ ligand is expected to have the least affinity for the UO_2^{2+} with a protonated carboxyl group in position C7 being the most comparable to the quinone group in position C5. To the contrary, the fully deprotonated PQQ ligand with a negatively charged carboxylate group in position C7 is poised to bind the electrophilic UO_2^{2+} better than the two neutral carbonyl groups.

TABLE 2. PQQ Binding Energies (kJ/mol) and Entropies (J/mol K) Calculated at BP86/LANL2DZ Level Using a Water−Continuum Model for Representative Complexation Equilibria (1)-(4)

	ΔE^a	ΔE_0^b	ΔH_{solute}	ΔS_{solute}	ΔG_{solute}	$\Delta G_{solution}^c$
$[UO_2(H_2O)_6]^{2+} + CO_3^{2-} \rightarrow [UO_2(CO_3)(H_2O)_3] + 3H_2O$ (1)						
	−180	−203	−187	297	−275	−255
$[UO_2(CO_3)(H_2O)_3] + PQQ^{3-} \rightarrow [UO_2(CO_3)(PQQ)(H_2O)]^{3-} + 2H_2O$ (2)						
[ONO]	−31	−39	−35	59	−53	−49
[OO]	11	8	5	−122	41	43
$[UO_2(CO_3)(H_2O)_3] + PQQ \rightarrow [UO_2(CO_3)(PQQ)(H_2O)] + 2H_2O$ (3)						
[ONO]	60	51	55	50	40	45
[OO]	45	44	44	−92	72	75
$[UO_2(CO_3)] +$ truncated PQQ $\rightarrow [UO_2(CO_3)$(truncated-PQQ)] (4)						
[NO]	−195	−188	−187	−187	−131	
[OO]	−163	−158	−156	−171	−105	

[a] Sum of nuclear/nuclear, electron/nuclear, and electron/electron interaction energies. [b] Zero-point energy corrected electronic energy (ΔE). [c] Corrected with nonelectrostatic solvent−solvent interaction term.

The displacement of three water molecules (equilibrium (1) in Table 2) by a bicarbonate (Figure 5b) in a coordinatively saturated, solvated UO_2^{2+} (Figure 5a) is a greatly spontaneous process, even when the penalty of solvent reorganization is considered ($\Delta G = -255$ kJ/mol). This corroborates the ESI-MS results showing the presence of a UO_2CO_3 species. The alternative reaction of displacement of only two water molecules to give the $[UO_2(CO_3)(H_2O)_4]$ complex (not shown) is more exothermic; however, the lower entropy gain makes this process less spontaneous ($\Delta G = -231$ kJ/mol) than shown for equilibrium (1) in Table 2.

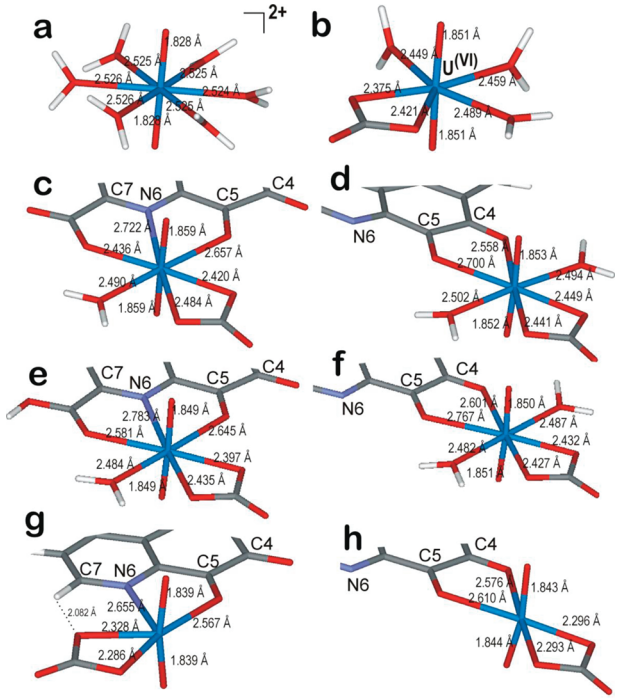

FIGURE 5. Optimized molecular structures for complexes in Table 2 with selected bond lengths for $[UO_2(H_2O)_6]^{2+}$ (a); $[UO_2(CO_3)(H_2O)_3]$ (b); $[UO_2(CO_3)([ONO]\text{-}PQQ)(H_2O)]^{3-}$ (c); $[UO_2(CO_3)([OO]\text{-}PQQ)(H_2O)_2]^{3-}$ (d); $[UO_2(CO_3)([ONO]\text{-}PQQ)(H_2O)]$ (e); $[UO_2(CO_3)([OO]\text{-}PQQ)(H_2O)_2]$ (f); $[UO_2(CO_3)([ON]\text{-truncated-}PQQ)]$ (g); $[UO_2(CO_3)([OO]\text{-truncated-}PQQ)]$ (h) complexes. For clarity, only the binding sites of interest of PQQ are shown.

For $[UO_2(CO_3)(H_2O)_x(PQQ)]$ complexes (Figure 5c−f), the coordinatively saturated complexes are the most stable (Equilibria 2−3 in Table 2) independently from the PQQ protonation state. Thus, UO_2^{2+} binding to PQQ via [ONO] and [OO] sites will displace two or one water molecules to give octacoordinate uranium complexes, respectively. Table 2 clearly indicates that the free energy of binding is considerably more negative for complexes where the PQQ ligand coordinated via the [ONO] site. The energetic differences between equilibria 2 and 3 indicate the likely presence of a considerable pH dependence of the PQQ complexation. The deprotonated PQQ binding is spontaneous ($\Delta G = -49$ kJ/mol), while upon protonation of all carboxylate groups this process becomes nonspontaneous to approximately the same extent ($\Delta G = 45$ kJ/mol).

Importantly, we also evaluated the most likely structure for the truncated PQQ species (Figure 5g and h) detected with $m/z = 527$. On the basis of stoichiometry and most reasonable fragmentation processes, this species can be best described above as a desolvated UO_2CO_3 coordinated with a triple decarboxylated PQQ cofactor. As shown for equilibrium 4 in Table 2, significant energetic difference was found between the coordination to the pyridine N and quinone oxygen ([NO]-coordination, Figure 5g) in the N6 and C5 positions, respectively, relative to the two quinone oxygens ([OO]-coordination, Figure 5h) in positions C5 and C4. This is likely due to the presence of a weak, yet significant C7−H...O hydrogen bonding interaction in addition to aromatic N being a better electron donor than a carbonyl O. Thus, these calculations indicate the preference of the same coordination mode for the truncated PQQ ligand detected in mass spectrometry measurements as for the intact PQQ ligand present in solution.

Biotic Ligand Model. As an extension of earlier results (*18*), the acute UO_2^{2+} toxicity demonstrated here is the result of specific physiological targeting of PQQ by UO_2^{2+} and is therefore consistent with the biotic ligand model (BLM) of acute metal toxicity. According to this model, metal toxicity patterns are the result of the presence of sensitive physiological binding targets and factors depending largely on the aqueous chemistry of the bulk system (*39, 40*). While previous studies incorporating the BLM have demonstrated the importance of bulk chemistry on UO_2^{2+} toxicity (*41*), the importance of physiological targeting has gone virtually unreported due to a lack of knowledge regarding specific targets susceptible to UO_2^{2+} binding. This study should therefore significantly expand the potential to apply the BLM to describe UO_2^{2+} toxicity.

Furthermore, these results also provide initial insights into the inhibition of bacterial Mn(II) oxidation in the presence of low UO_2^{2+} concentrations as proposed earlier (*7*). On the basis of similarity in the binding sites of Ca^{2+} and UO_2^{2+}, we suggest that UO_2^{2+} ions may also coordinate with enzymes or enzyme cofactors responsible for Mn(II) oxidation. The potential ability of UO_2^{2+} to directly inhibit biogenic Mn-oxide formation may point to limitations for using biological, Mn-based permeable reactive barriers in UO_2^{2+} bioremediation schemes. The structural results obtained for UO_2^{2+} substantiate its versatile coordination chemistry via a pyridine N and a quinone oxygen separated by two atoms, as these render UO_2^{2+} to be a potential inhibitor of flavoproteins that occur in higher organisms, including humans. Ongoing work includes whole cell inhibition of *Methylobacterium extorquens* AM1during aerobic growth on methanol, which is also PQQ-dependent (*42*). Future work could also focus on studying direct enzymatic inhibition by UO_2^{2+}, thus bridging the gap between whole cell and molecular studies.

Acknowledgments

The authors at MSU gratefully acknowledge the financial support provided by the U.S. Department of Energy, Office of Science, Environmental Remediation Science Program (ERSP) contract DE-FG02-06ER64206. The INL portion of the work was supported by the U.S. Department of Energy, Assistant Secretary for the Office of Science, ERSP, under DOE-NE Idaho Operations Office contract number DE-AC07-05ID14517. Laboratory facilities and support was provided by the Chemical and Biological Engineering Department and the Center for Biofilm Engineering at Montana State University. The authors acknowledge funding for the establishment of the Environmental and Biofilm Mass Spectrometry Facility at MSU through the Defense University Research Instrumentation Program (DURIP, Contract Number: W911NF0510255). Funding for computational resources was provided by the MSU Center for Bio-Inspired Nanomaterials (ONR N0014-07-1-0645).

Literature Cited

(1) Landa, E. R.; Gray, J. R. US Geological Survey—Research on the environmental fate of uranium mining and milling wastes. *Environ. Geol.* **1995**, *26*, 19–31.
(2) Parrish, R. R.; Horstwood, M.; Arnason, J. G.; Chenery, S.; Brewer, T.; Lloyd, N. S.; Carpenter, D. O. Depleted uranium contamination by inhalation exposure and its detection after similar to 20 years: Implications for human health assessment. *Sci. Total Environ.* **2008**, *390*, 58–68.
(3) Milačić, S.; Petrović, D.; Jovičić, D.; Kovačević, R.; Simić, J. Examination of the health status of populations from depleted-uranium-contaminated regions. *Environ. Res.* **2004**, *95*, 2–10.
(4) Riley, R. G.; Zachara, J. DOE/ER-0547T; U.S. Department of Energy: Washington, DC, 1992.
(5) Wall, J. D.; Krumholz, L. R. Uranium reduction. *Ann. Rev. Microbiol. 60*, **2006**, 149−166.
(6) Appukuttan, D.; Rao, A. S.; Apte, S. K. Engineering of *Deinococcus radiodurans* R1 for bioprecipitation of uranium from dilute nuclear waste. *Appl. Environ. Microbiol.* **2006**, *72*, 7873–7878.

(7) Webb, S. M.; Fuller, C. C.; Tebo, B. M.; Bargar, J. R. Determination of uranyl incorporation into biogenic manganese oxides using X-ray absorption spectroscopy and scattering. *Environ. Sci. Technol.* **2006**, *40*, 771–777.
(8) Chinni, S.; Anderson, C. R.; Ulrich, K. U.; Giammar, D. E.; Tebo, B. M. Indirect UO_2 Oxidation by Mn(II)-oxidizing Spores of *Bacillus* sp. strain SG-1 and the effect of U and Mn concentrations. *Environ. Sci. Technol.* **2008**, *42*, 8709–8714.
(9) Johnson, H. A.; Tebo, B. M. In vitro studies indicate a quinone is involved in bacterial Mn(II) oxidation. *Arch. Microbiol.* **2008**, *189*, 59–69.
(10) Matsushita, K.; Toyama, H.; Yamada, M.; Adachi, O. Quinoproteins: Structure, functions and biotechnological applications. *Appl. Microbiol. Biotechnol.* **2002**, *58*, 13–22.
(11) Manceau, A.; Gorshkov, A. I.; Drits, V. A. Structural chemistry of Mn, Fe, Co, and Ni in manganese hydrous oxides 2. Information from EXAFS spectroscopy and electron and X-ray-diffraction. *Am. Mineral.* **1992**, *77*, 1144–1157.
(12) Davis, J. A.; Curtis, G. P. *NUREG/CR-6820*; U.S. Nuclear Regulatory Commission: Washington, DC, 2003.
(13) Kasahara, T.; Kato, T. A new redox-cofactor vitamin for mammals. *Nature* **2003**, *422*, 832.
(14) Felton, L. M.; Anthony, C. Role of PQQ as a mammalian enzyme cofactor. *Nature* **2005**, *433*, E10.
(15) Bastide, P. J.; Bastide, P. 5-Hydroxytryptophan-decarboxylase and monoamine oxidase activities in kidneys of rats and mice after experimental uranyl nitrate intoxication. *Ann. Biol. Clin.* **1968**, *26*, 1239–1245.
(16) Zheng, Y. J.; Bruice, T. C. Conformation of coenzyme pyrroloquinoline quinone and role of Ca^{2+} in the catalytic mechanism of quinoprotein methanol dehydrogenase. *Proc. Natl. Acad. Sci. U.S.A.* **1997**, *94*, 11881–11886.
(17) Schürer, G.; Clark, T. Is the calcium-ion catalysis of biological reoxidation of reduced PQQ purely electrostatic? *Chem. Commun.* **1998**, 257–258.
(18) VanEngelen, M. R.; Field, E. K.; Gerlach, R.; Lee, B. D.; Apel, W. A.; Peyton, B. M. UO_2^{2+} speciation determines uranium toxicity and bioaccumulation in an environmental *Pseudomonas* sp. isolate. *Environ. Toxicol. Chem.* **2010**, *29*, 763–769.
(19) Wu, W. M.; Hickey, R. F.; Zeikus, J. G. Characterization of metabolic performance of methanogenic granules treating brewery wastewater: role of sulfate-reducing bacteria. *Appl. Environ. Microbiol.* **1991**, *57*, 3438–3449.
(20) Becke, A. D. Density-functional exchange-energy approximation with correct asymptotic-behavior. *Phys. Rev. A* **1988**, *38*, 3098–3100.
(21) Perdew, J. P. Density-functional approximation for the correlation-energy of the inhomogeneous electron-gas. *Phys. Rev. B* **1986**, *33*, 8822–8824.
(22) Hay, P. J.; Wadt, W. R. Ab initio effective core potentials for molecular calculations—Potentials for the transition-metal atoms Sc to Hg. *J. Chem. Phys.* **1985**, *82*, 270–283.
(23) Hay, P. J.; Wadt, W. R. Ab initio effective core potentials for molecular calculations—Potentials for K to Au including the outermost core orbitals. *J. Chem. Phys.* **1985**, *82*, 299–310.
(24) Tomasi, J.; Persico, M. Molecular interactions in solution: An overview of methods based on continuous distributions of the solvent. *Chem. Rev.* **1994**, *94*, 2027–2094.
(25) Cossi, M.; Barone, V.; Cammi, R.; Tomasi, J. Ab initio study of solvated molecules: A new implementation of the polarizable continuum model. *Chem. Phys. Lett.* **1996**, *255*, 327–335.
(26) Frisch, M. J.; Trucks, G. W.; Schlegel, H. B.; Scuseria, G. E.; Robb, M. A.; Cheeseman, J. R.; Montgomery, J. A., Jr.; Vreven, T.; Kudin, K. N.; Burant, J. C.; Millam, J. M.; Iyengar, S. S.; Tomasi, J.; Barone, V.; Mennucci, B.; Cossi, M.; Scalmani, G.; Rega, N.; Petersson, G. A.; Nakatsuji, H.; Hada, M.; Ehara, M.; Toyota, K.; Fukuda, R.; Hasegawa, J.; Ishida, M.; Nakajima, T.; Honda, Y.; Kitao, O.; Nakai, H.; Klene, M.; Li, X.; Knox, J. E.; Hratchian, H. P.; Cross, J. B.; Bakken, V.; Adamo, C.; Jaramillo, J.; Gomperts, R.; Stratmann, R. E.; Yazyev, O.; Austin, A. J.; Cammi, R.; Pomelli, C.; Ochterski, J. W.; Ayala, P. Y.; Morokuma, K.; Voth, G. A.; Salvador, P.; Dannenberg, J. J.; Zakrzewski, V. G.; Dapprich, S.; Daniels, A. D.; Strain, M. C.; Farkas, O.; Malick, D. K.; Rabuck, A. D.; Raghavachari, K.; Foresman, J. B.; Ortiz, J. V.; Cui, Q.; Baboul, A. G.; Clifford, S.; Cioslowski, J.; Stefanov, B. B.; Liu, G.; Liashenko, A.; Piskorz, P.; Komaromi, I.; Martin, R. L.; Fox, D. J.; Keith, T.; Al-Laham, M. A.; Peng, C. Y.; Nanayakkara, A.; Challacombe, M.; Gill, P. M. W.; Johnson, B.; Chen, W.; Wong, M. W.; Gonzalez, C.; Pople, J. A. *Gaussian 03*, revision C.02; Gaussian, Inc.: Wallingford, CT, 2004.
(27) Goodwin, P. M.; Anthony, C. *The Biochemistry, Physiology and Genetics of PQQ and PQQ-Containing Enzymes*; Poole, R. K., Ed.; Academic Press: San Diego, CA, 1998.
(28) Masgrau, L.; Basran, J.; Hothi, P.; Sutcliffe, M. J.; Scrutton, N. S. Hydrogen tunneling in quinoproteins. *Arch. Biochem. Biophys.* **2004**, *428*, 41–51.
(29) Kay, C. W. M.; Mennenga, B.; Görisch, H.; Bittl, R. Substrate binding in quinoprotein ethanol dehydrogenase from *Pseudomonas aeruginosa* studied by electron-nuclear double resonance. *Proc. Natl. Acad. Sci. U.S.A.* **2006**, *103*, 5267–5272.
(30) Itoh, S.; Kawakami, H.; Fukuzumi, S. Modeling of the chemistry of quinoprotein methanol dehydrogenase. Oxidation of methanol by calcium complex of coenzyme PQQ via addition-elimination mechanism. *J. Am. Chem. Soc.* **1997**, *119*, 439–440.
(31) Dimitrijevic, N. M.; Poluektov, O. G.; Saponjic, Z. V.; Rajh, T. Complex and charge transfer between TiO_2 and pyrroloquinoline quinone. *J. Phys. Chem. B* **2006**, *110*, 25392–25398.
(32) Noji, N.; Nakamura, T.; Kitahata, N.; Taguchi, K.; Kudo, T.; Yoshida, S.; Tsujimoto, M.; Sugiyama, T.; Asami, T. Simple and sensitive method for pyrroloquinoline quinone (PQQ) analysis in various foods using liquid chromatography/electrospray-lonization tandem mass spectrometry. *J. Agric. Food Chem.* **2007**, *55*, 7258–7263.
(33) Guillaumont, R. *Chemical Thermodynamics Vol. 5: Update on the Chemical Thermodynamics of Uranium, Neptunium, Plutonium, Americium, And Technetium*; Elsevier B. V.: Amsterdam, The Netherlands, 2003.
(34) Baston, G. M. N.; Berry, J. A.; Bond, K. A.; Boult, K. A.; Brownsword, M.; Linklater, C. M. Effects of cellulosic degradation products on uranium sorption in the geosphere. *J. Alloy. Compd.* **1994**, *213*, 475–480.
(35) Allen, F. H. The Cambridge Structural Database: A quarter of a million crystal structures and rising. *Acta Crystallogr.* **2002**, *B58*, 380–388.
(36) Ishida, T.; Doi, M.; Tomita, K.; Hayashi, H.; Inoue, M.; Urakami, T. Molecular and crystal structure of PQQ (methoxatin), a novel coenzyme of quinoproteins—Extensive stacking character and metal-ion interaction. *J. Am. Chem. Soc.* **1989**, *111*, 6822–6828.
(37) Wanner, M.; Sixt, T.; Klinkhammer, K. W.; Kaim, W. First experimental structure of a 1: 1 metal complex with a PQQ cofactor derivative outside dehydrogenase enzymes. *Inorg. Chem.* **1999**, *38*, 2753–2755.
(38) Nakamura, N.; Kohzuma, T.; Kuma, H.; Suzuki, S. Synthetic and structural studies on copper(II) complexes containing coenzyme PQQ and terpyridine. *Inorg. Chem.* **1994**, *33*, 1594–1599.
(39) Di Toro, D. M.; Allen, H. E.; Bergman, H. L.; Meyer, J. S.; Paquin, P. R.; Santore, R. C. Biotic ligand model of the acute toxicity of metals. 1. Technical basis. *Environ. Toxicol. Chem.* **2001**, *20*, 2383–2396.
(40) Niyogi, S.; Wood, C. M. Biotic ligand model, a flexible tool for developing site-specific water quality guidelines for metals. *Environ. Sci. Technol.* **2004**, *38*, 6177–6192.
(41) Alves, L. C.; Borgmann, U.; Dixon, D. G. Water-sediment interactions for *Hyalella azteca* exposed to uranium-spiked sediment. *Aquat. Toxicol.* **2008**, *87*, 187–199.
(42) Nunn, D. N.; Day, D.; Anthony, C. The second subunit of methanol dehydrogenase of *Methylobacterium extorquens* AM1. *Biochem. J.* **1989**, *260*, 857–862.

ES101754X